



OPTICAL SPECTROSCOPY OF SDSS J004054.65-0915268: THREE POSSIBLE SCENARIOS FOR THE CLASSIFICATION. A $z \sim 5$ BL LACERTAE, A BLUE FSRQ, OR A WEAK EMISSION LINE QUASAR

M. LANDONI & A. ZANUTTA,

AND A. BIANCO, F. TAVECCHIO, G. BONNOLI, AND G. GHISELLINI
INAF-Osservatorio Astronomico di Brera, Via Emilio Bianchi 46, I-23807 Merate, Italy
Received 2015 February 20; accepted 2015 December 15; published 2016 January 28

ABSTRACT

The hunt of high-redshift BL Lacertae objects is day by day more compelling to firmly understand their intrinsic nature and evolution. SDSS J004054.65-0915268 is, at the moment, one of the most distant BL Lac candidates, at $z \sim 5$. We present a new optical-near-IR spectrum obtained with ALFOSC-NOT with a new, custom designed dispersive grating aimed to detect broad emission lines that could disprove this classification. In the obtained spectra, we do not detect any emission features and we provide an upper limit to the luminosity of the C IV broad emission line. Therefore, the nature of the object is then discussed, building the overall spectral energy distribution (SED) and fitting it with three different models. Our fits, based on SED modeling with different possible scenarios, cannot rule out the possibility that this source is indeed a BL Lac object, though the absence of optical variability and the lack of strong radio flux seem to suggest that the observed optical emission originates from a thermalized accretion disk.

Key words: BL Lacertae objects: general – techniques: imaging spectroscopy

1. INTRODUCTION

BL Lac objects are active galactic nuclei dominated by a strongly beamed nuclear non-thermal emission arising in a relativistic jet pointed toward the Earth (e.g., Urry & Padovani 1995). Relativistic effects amplify the radiation produced in the jet by relativistic electrons through synchrotron and inverse Compton mechanisms. Moreover, contrary to a flat spectrum radio quasar, the intrinsic nuclear thermal components are also quite weak (e.g., Ghisellini et al. 2011). As a consequence, the non-thermal continuum outshines spectral features (emissions of absorptions), making the determination of their redshift quite tricky (Landoni et al. 2013, 2015). Nevertheless, the estimate of their distance is obviously important to shed light on the nature of their radiation mechanism and about their evolution. In fact, radio-selected BL Lacs display moderate positive evolution, while X-ray-selected objects negatively evolve when derived from X-ray surveys, or do not evolve at all (Rector et al. 2000; Padovani et al. 2007; Giommi et al. 2009, 2012). A continuum trend from slightly positive evolution for low energy peaked BL Lacs, to strong negative evolution in the case of high-peaked ones was proposed (Rector et al. 2000). However, the statistics concerning the evolution of the BL Lacs suffer from redshift incompleteness, making the increase of the objects with reliable redshifts (from homogeneous and unbiased selections) a core issue (see also Shaw & Romani 2013 for a discussion). A more intriguing fact is that these objects are detected almost in the low- z universe ($z \leq 1$) and very few sources are known at $z \geq 2$ (see, e.g., Shaw & Romani 2013). This has been interpreted in terms of the evolution from highly accreting sources (FSRQ) to BL Lacs, in which accretion is rather low (Böttcher & Dermer 2002; Cavaliere & D’Elia 2002).

For all of these reasons, the search of high-redshift BL Lacs is becoming even more compelling. With this aim, we searched in the most extensive BL Lac catalogs to find high- z candidate sources, focusing on the compilation of the homogeneous optically selected BL Lac objects from the Sloan Digital Sky Survey by Plotkin et al. (2010). We found that, in the sample of

radio-loud BL Lac candidates, the source SDSS J004054.65-0915268 (hereafter 0040–0915) is characterized by a featureless optical continuum and its redshift, based on a Lyman-limit system (LLS), is surprisingly high ($z = 4.976$), making it one of the most distant BL Lac candidates. It is worth mentioning that Fan et al. (2006) serendipitously found another, even more distant, candidate BL Lac object (but see Leipski et al. 2014 classifying it as QSO). However, the required spectral range to reveal broad emission lines redward of the Ly α line, such as the C IV, is unfortunately outside the sensitivity range of our instrument in this object. For this reason, we thus select 0040–0915 for our spectroscopic investigation, whose nature is a matter of debate in the literature. In fact, while Collinge et al. (2005) and Plotkin et al. (2010) consider the source to be a BL Lac candidate (see Table 5 in both papers), Lane et al. (2011) on the basis of *Spitzer* mid-IR data suggest that the source is not dominated by non-thermal continuum, challenging the BL Lac hypothesis. This source has been considered to be a weak emission line quasar (WELQ), a new recent class of AGNs with weak or absent broad emission lines, by Diamond-Stanic et al. (2009). Despite having only an upper limit in the radio band, it was classified as a Radio Loud BL Lac Candidate object by Plotkin et al. (2010). The different classifications of this source rely mainly on the SDSS spectrum, which, unfortunately, can determine only the presence or absence of the broad Ly α line. This spectral feature could be weak for the combination of both severe intervening absorptions or a poor SNR in that band.

In the SDSS spectrum of 0040–0915, the Ly α emission line appears to be absent while other weak features could be interpreted as S IV or N V emission. We note, however, that a proper modeling of the continuum and emission line should be used to robustly infer the detection of the feature. However, the poor signal-to-noise ratio of the SDSS spectrum does not allow us to further speculate on those emission lines. The C IV broad emission line, whose detection allows us to disentangle between scenarios, could be only partially detected near the end of the spectral range (in the near-IR band). For all of these

Table 1
Grism #20 Main Specifications' Summary

GRISM Name	λ_{central} (Å) (1)	Efficiency at 7350 Å (2)	Dispersion (Å pixel ⁻¹) (3)	$\Delta\lambda$ (Å) (4)	Resolution (5)	1/mm (6)
Grism #20	7350	88%	2.079	5760–10200	895	484

Note. Col. (1): working central wavelength of the grating; Col. (2): device's first order diffracted efficiency; Col. (3): pixel dispersion of the grism; Col. (4): wavelength range; Col. (5): calculated resolution; Col. (6): pitch of the grating.

Table 2
Model Parameters and Derived Values for the Three considered Scenarios

Name [1]	M_{BH} [2]	Γ [3]	θ_v [4]	R_{diss} [5]	R_{BLR} [6]	P'_r [7]	B [8]	γ_b [9]	γ_{max} [10]	α_X [11]	E_c [12]
Radio-quiet	2e9	1132	1.2	130
Blue FSRQ	1e9	14	3	360	212	4e-3	1.2	1.5e4	1e6	1.2	150
BL Lac	...	14	3	240	...	3e-3	1	1.4e4	1e6	1.	...

Notes. Col. [1]: type of source; Col. [2]: black hole mass in solar mass units; Col. [3]: bulk lorentz factor; Col. [4]: viewing angle (degrees); Col. [5]: distance of the blob from the black hole in units of 10^{15} cm; Col. [6]: size of the broad line region in units of 10^{15} cm; Col. [7]: power injected in the blob calculated in the comoving frame, in units of 10^{45} erg s⁻¹; Col. [8]: magnetic field in gauss; Col. [9] and [10]: minimum and maximum random Lorentz factors of the injected electrons; Col. [10]: energy spectral index assumed for the X-ray corona; Col. [11]: cut-off energy of the X-ray spectrum, in keV [assumed to be]

reasons, a good quality near-IR spectrum largely covering the region of the expected C IV feature (up to 1 μm) is mandatory to possibly firmly detect the line and clear the fog surrounding the scenario between normal broad line QSO, BL Lac, or exotic source.

In order to fill this gap, we exploited the upgrade of the dispersive element at the Andalucia Faint Object Spectrograph and Camera (ALFOSC) spectrograph at the Nordic Optical Telescope (NOT, La Palma, ES), designing a new red grating to match these particular requirements aiming to perform the needed observation. Although in the literature there are a number of papers that discuss the existence of quasars with weak emission lines (see, e.g., Diamond-Stanic et al. 2009; Plotkin et al. 2010; Lane et al. 2011; Meusinger et al. 2014), no exhaustive broadband spectral energy distributions (SEDs) are interpreted adopting various models, ranging from normal QSO to BL Lacs. In particular, in this work, we present SEDs assembled with data from far-IR to X-Rays data and we apply physical models to possibly shed light on the nature of the source. In this paper, we thus show both the obtained spectroscopic results along with three possible frameworks for the interpretation of this high-redshift source by the adoption of popular scenarios (see, e.g., Ghisellini et al. 1996; Maraschi et al. 2010).

The paper is organized as follow. We report, in Section 2, the grating manufacturing and the data reduction while main results are reported in Section 3. Discussion and conclusions are given in the last section. We use cgs units unless stated otherwise and the following cosmological parameters, $H_0 = 70 \text{ km s}^{-1} \text{ Mpc}^{-1}$, $\Omega_m = 0.27$, $\Omega_\Lambda = 0.73$.

2. GRATING MANUFACTURING, OBSERVATIONS, AND DATA REDUCTION

The dispersive element used for the spectroscopic acquisition highlighted in this work was specifically designed and produced in the INAF (OABr, Merate) facilities. The possibility to design and manufacture a dispersive element specific for a target observation is surely effective for

Table 3
Model Parameters and Derived Values for the Three considered Scenarios

Name [1]	$\log L_d$ [2]	L_d/L_{Edd} [3]	$\log P_r$ [4]	$\log P_B$ [5]	$\log P_e$ [6]	$\log P_p$ [7]
Radio-quiet	47	0.45
blue FSRQ	46	0.03	45	45	44	44
BL Lac	45	45	44	44

Notes. Accretion and jet powers: Col. [1]: type of source; Col. [2]: logarithm of the accretion disk luminosity (units are erg s⁻¹); Col. [3]: accretion disk luminosity in eddington units; Col. [4]–[7]: logarithm of the jet power in the form of radiation (P_r), poynting flux (P_B), bulk motion of electrons (P_e) and [7] protons (P_p), assuming one cold proton per emitting electron. units are erg s⁻¹. These values refer to two Jets

addressing future astronomical scientific cases. The logic behind this new custom device was to obtain a low dispersive element with an extended wavelength range, which is capable of detecting the C IV broadband line of the object 0040–0915. This device, called Grism #20, was integrated at NOT-ALFOSC and its specifications are reported in Table 1.

This dispersive element is a grism (GRating + pRISM), based on a volume phase holographic grating (VPHG) and manufactured with state-of-the-art photopolymeric material (Bayfol® HX), developed by Bayer MaterialScience AG (Berneth et al. 2013). Such photopolymers show an easy processability (they are self-developing) together with a large modulation of the refractive index (Δn) and, even more interesting, the Δn can be finely tuned by acting on the writing conditions. These materials are becoming a reliable alternative to dichromated gelatin (DCG, the reference material for VPHGs), with high dynamic range and sensitivity (Zanutta et al. 2014a, 2014b).

We delivered the grating at ALFOSC-NOT on 2014 September 27 and we observed 0040–0915 during the night of 2014 September 30 and October 1. We secured two individual exposures of 2200 s each using the 1''/8 slit. The seeing during the night was $\sim 1''/50$ and the sky was almost

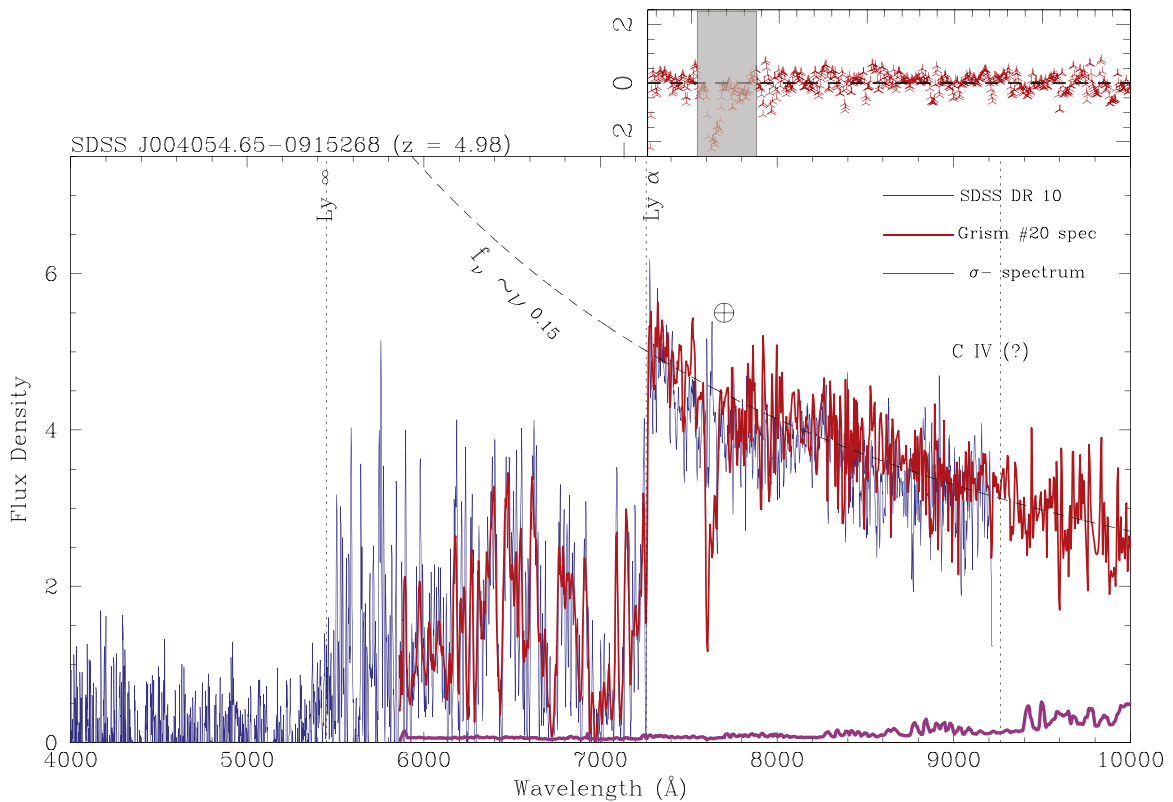


Figure 1. SDSS J004054.65-0915268 optical spectrum in the band $4000 \text{ \AA} - 1 \mu\text{m}$. Units are in $10^{-17} \text{ erg cm}^{-2} \text{ s}^{-1} \text{ \AA}^{-1}$. The blue solid line is the spectrum available in the Sloan Digital Sky Survey DR10 while the red solid line represents the newly acquired spectrum at ALFOSC-NOT. Telluric absorption lines are marked with \oplus . The redshift of the source, estimated through $\text{Ly}\alpha$ break and Lyman-limit features, is $z = 4.981$. The presence of broad emission lines ascribed to $\text{Ly}\alpha$ and C IV is ruled out up to $\text{EW} \sim 5 \text{ \AA}$. The dashed black line is the continuum best fit ($F(\nu) \propto \nu^{0.15}$). The purple solid line is the 1σ spectrum. Upper right panel: residual between the fit and the observed NOT spectrum.

clear. We also observed two standard stars with the same configuration of the instrument to flux calibrate the two spectra. Standard IRAF¹ procedures were adopted (bias, flat field correction, wavelength, and flux calibration) to fully reduce each observation. Finally, we averaged the two spectra according to their signal-to-noise ratios ($S/N \sim 15$) in order to obtain the mono-dimensional spectrum. We also cross-checked the absolute flux calibration through an aperture photometry of the i-band acquisition image of the field, secured just before obtaining the spectra.

3. RESULTS

We report in Figure 1 the optical spectrum of 0040-0915 obtained by the SDSS DR10 (blue solid line) and the new one secured with ALFOSC-NOT equipped with Grism #20 (red solid line, $\text{SNR} \sim 15$). The redshift of the source, estimated through the $\text{Ly}\alpha$ brake and the Lyman limit, is $z \sim 4.981$ and no intrinsic broad emission lines (neither $\text{Ly}\alpha$ nor C IV) are detected. We mark in Figure 1 the expected position of the C IV emission line at the redshift mentioned above ($\lambda \sim 9300$) with a vertical dotted line. We fitted the continuum by the adoption of a power law of the form $f_\nu \propto \nu^{0.15}$, consistent with the results obtained by Fan et al. (2006) for a similar high- z lineless AGN (see Figure 3 of Fan et al. 2006). Residuals are reported in the

top right panel of Figure 1. The SDSS spectrum, due to its poor S/N at the edge of spectral sensitivity and its short range in the near-IR (see Figure 1) cannot rule out the presence of a broad emission line ascribed as C IV. We note, however, that the SDSS best fit reported in DR10 could have been tumbled a possible weak emission of $\text{Ly}\alpha$, though in that region the fit is rather poor and systematically underestimates the continuum. This hint is not, however, detected in our newly obtained spectra (see Figure 1). In fact, the fit adopted by the SDSS could mimic the presence of spectral features that are not obviously present in the data. For instance, the detection of the S IV emission line has been ruled out in the new DR10 release.

3.1. C IV Equivalent Width Upper Limit

The ALFOSC-NOT spectrum, which extends up to $1 \mu\text{m}$, has a sufficient spectral coverage and decent S/N to safely exclude the presence of the C IV broad emission line (see Figure 1). Following the description by Fan et al. (2006), we modeled the spectrum in region 8000–10,000 (where the S/N and resolution can be considered roughly constant for our estimation) using the power law described before plus an emission line model ($\text{FWHM} \sim 3000\text{--}4000 \text{ km s}^{-1}$) for the C IV and applying to the resulting model an S/N similar to that observed in the NOT spectrum. We performed simulations by increasing the Equivalent Width (EW) of the line until the signal in the simulated spectrum exceeds the noise by 3σ . We repeated this recipe 100 times, as in a usual Monte Carlo simulation.

¹ IRAF (Image Reduction and Analysis Facility) is distributed by the National Optical Astronomy Observatories, which are operated by the Association of Universities for Research in Astronomy, Inc., under cooperative agreement with the National Science Foundation.

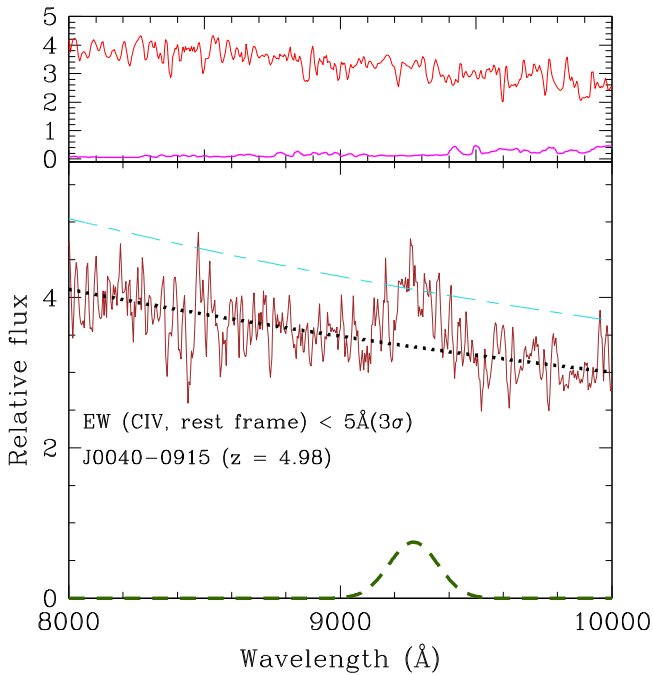


Figure 2. C IV emission line equivalent width limit estimation. In the bottom panel is reported the simulated spectrum by the adoption of the power law (dotted black line, estimated on the NOT spectrum) and a C IV emission line model with EW of 5 Angstrom rest frame (dark green dashed line) and an FWHM of 4000 km s^{-1} rest frame. The resulting spectrum, which is the sum of the component plus a noise to simulate the same SNR of the NOT spectrum, is indicated by the solid brown line. The 3σ threshold is indicated by the light blue dashed line. Upper panel: Comparison of the observed NOT spectrum (solid red) and the 1σ error spectrum (solid purple line). Details on the estimation are given in the paper.

We report, in Figure 2, the results obtained from this procedure. We show in the lower panel the two components of the model (dotted line for the power law and dashed line for the line) and the resulting spectrum (brown solid line) after applying Gaussian noise to simulate our observed S/N. Since the C IV emission line has a rest frame EW of 5 \AA and its signal exceeds the noise with a threshold level of $3\text{-}\sigma$ we can conclude that the upper limit to the EW of C IV is 5 \AA at a 3σ confidence level. For comparison, we report in the upper panel the observed NOT spectrum (red) and the 1σ error spectrum (purple solid line). As a sanity check, we also calculated the minimum equivalent width in the same region following the procedure described in Sbarufatti et al. (2006) and adopted in various papers to assess limits on the detectability of spectral features (see, e.g., Schneider et al. 1993; Sbarufatti et al. 2006; Farina et al. 2013). This method is completely model independent and relies only on the width of the spectral element (which is a function of the instrument) and the S/N (see Sbarufatti et al. 2006 for details). In particular, we evaluated the EW on bins of the size of the resolution element in various regions of the spectrum (excluding the telluric structures) and we assume as EW_{\min} the 3σ deviation from the mean ($\mu \sim 0 \text{ \AA}$) of the distribution of the EWs obtained in each bin. We found that the EW_{\min} (rest frame) is $\sim 5 \text{ \AA}$ consistent with the limit obtained with the model described above. We can thus conclude that, if the C IV feature is present, it shall have an $\text{EW} \leq 5 \text{ \AA}$ rest frame. We report in the following section the possible scenarios that could explain the observed optical-near-

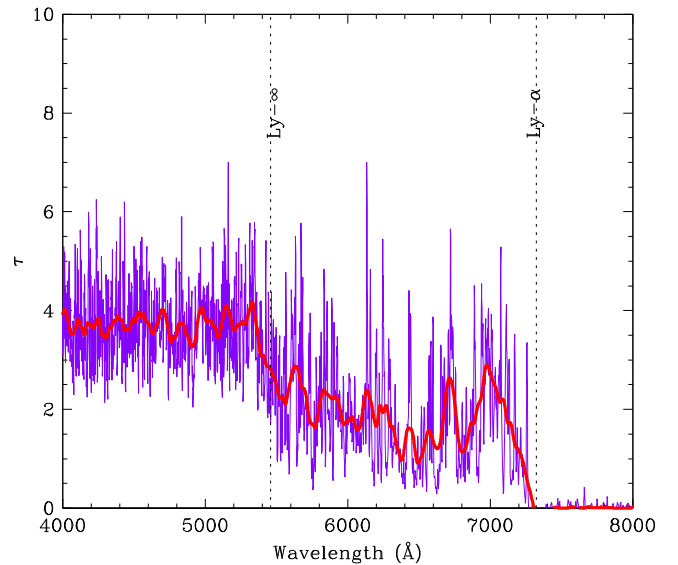


Figure 3. Optical depth derived from the spectrum of 0040-0915. The blue solid line is the ratio between the observed flux on the SDSS spectrum and the intrinsic one extrapolated from the power-law fit (see Section 3.2). The thick solid line is a 20 \AA boxcar filter on the blue spectrum. The redshift of the nearest H I cloud is assessed through the wavelength where the optical depth drops to $\tau \sim 0$. This value catches the cold H I cloud nearest to 0040-915. The expected position of the Lyman- ∞ is consistent with our interpretation (see the text of Section 3.2) and it is marked with a vertical dotted line.

IR spectrum after a discussion regarding caveats of the estimation of the source’s redshift.

3.2. Caveats on the Redshift of 0040-0915

The redshift estimation from the onset of the Ly α forest can be biased to higher values (up to $\Delta z \sim 0.1$) if the EW of the broad Ly α line is very small (see, e.g., Figure 3 of Diamond-Stanic et al. 2009). Although in the NOT and SDSS spectra the continuum appears to be dominated by the power-law component and this effect could be mitigated, other biases should be considered when redshift is derived only through absorption features (see, e.g., Prochaska et al. 2008 and Figures 1 and 2 in Steidel et al. 2010). In particular, the onset of the Ly α forest can be affected by absorption both blueward and redward of the Ly α emission line. When considering systems like proximate Damped Ly α System (Prochaska et al. 2008) absorptions near the systemic velocity that completely absorbs the center of the Ly α line could move the onset of the Lyman forest toward redder wavelengths. Overall, these effects can bias the observed redshift up to $\Delta z \sim 0.01$.

We tried to check the redshift of 0040-0915 through an alternative method based on the optical depth. Following Fan et al. (2006), we defined the optical depth as $\tau = -\log \frac{f_{\text{obs}}}{f_{\text{int}}}$ where f_{obs} is the observed flux of the source and f_{int} is the extrapolated intrinsic flux obtained from the power-law fit. We report the results (using the SDSS spectrum) in Figure 3. The wavelength location of $\tau = 0$ marks the 1216 \AA features, which correspond to $z = 4.989$. This value is consistent with the one considered in this paper and confirmed in the SDSS DR10 spectrum analysis ($z = 5.002$). Consistently, we also mark the position of the Lyman edge at 912 \AA at that redshift. As expected, at that location the optical depth monotonically increases up to the saturation plateau at $\tau \sim 4$ (see, e.g., Peterson 1997).

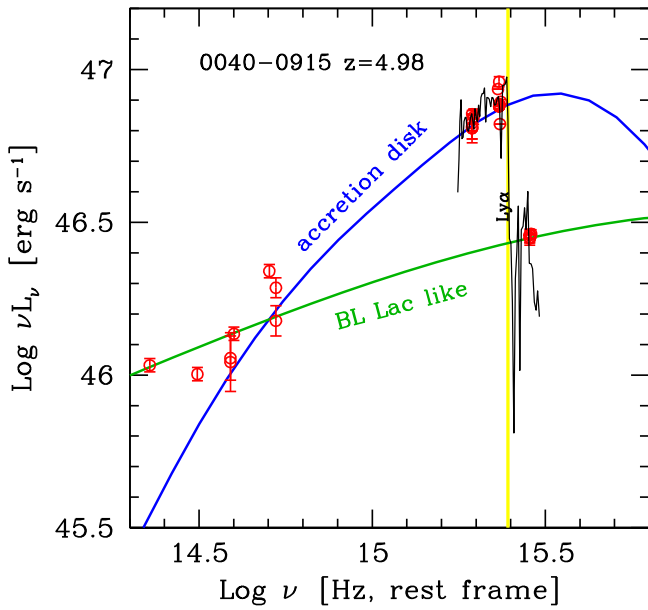


Figure 4. IR-optical SED of 0040–0915 in the rest frame. The archival photometry data (from SDSS, *WISE*, and *Spitzer*/IRAC) are red circles while our optical spectrum is the solid black line. The vertical yellow line indicates the hydrogen Ly α frequency. Above this line, we expect absorption due to intervening matter. The SED is compared with two different models: the solid blue line is the spectrum from a standard Shakura & Sunjaev (1973) disk, while the solid green line is the non-thermal continuum produced by a relativistic jet that fits the overall SED (as illustrated in Figure 5 in the mid and bottom panels).

4. DISCUSSION

The rest frame near-IR UV SED of 0040–0915 is shown in Figure 4, reporting archival data² and our spectrum, and in Figure 5, reporting the overall SED compared with three different models.

Weak or absent broad emission lines is the main defining property of BL Lac objects, namely jetted sources whose jets are pointing at us and whose jet emission is strongly boosted by the bulk relativistic motion of the emitting plasma. On the other hand, *all* known BL Lac objects are radio-emitters, as expected in the case of a jetted source. The other property of BL Lac objects pertinent to our case is the absence of visible accretion disk emission. Our source, instead, has a IR-optical SED showing a peak (in νL_ν) at a rest frame frequency in the UV band, and a rather hard spectrum below. The classification of 0040–0915 is, therefore, a puzzle. In the following, we interpret 0040–0915 alternatively as a radio-quiet quasar, a flat spectrum radio quasar (FSRQ) with a particularly enhanced and blue jet emission, and a BL Lac object.

The adopted model for the disk and jet emission is described in Ghisellini & Tavecchio (2009) (see also the discussion (Section 4) and Tables 2 & 3). We summarize here its main features and parameters. The disk is a standard Shakura-Sunjaev (1973) disk, with an X-ray corona phenomenologically described as emitting a cut-off power-law spectrum: $F_{\text{corona}}(\nu) \propto \nu^{-\alpha_x} \exp(-\nu/\nu_c)$. The non-thermal source is assumed to be a sphere located in the jet at some distance R_{diss} from the black hole. It is embedded in a homogeneous and

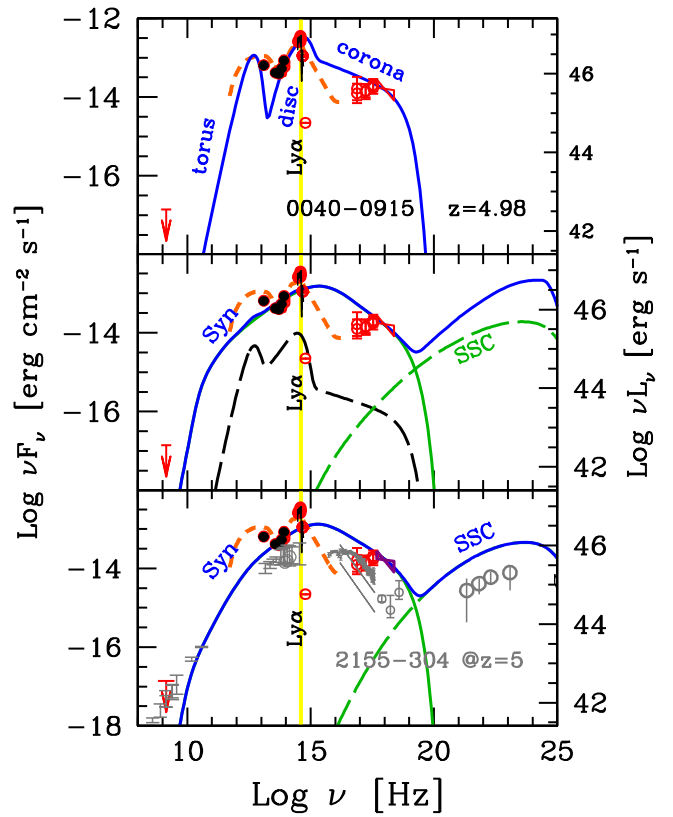


Figure 5. Spectral energy distribution of 0040–0915, interpreted with three different models. In all panels, the vertical yellow stripe indicates the location of the hydrogen Ly α line. Top panel: the source is assumed to be a radio-quiet quasar, whose accretion disk, torus, and X-ray corona are responsible for all data points. In this case, the anomaly of the source is the presence of a strong ionizing continuum produced by the disk without the corresponding presence of a “normal” broad line region. Mid panel: the source is assumed to be a “blue quasar,” namely a radio-loud FSRQ whose non-thermal jet emission overwhelms the thermal disk radiation. This implies a rather “blue” jet spectrum (Ghisellini et al. 2012). In this case, the broad lines, though present, are hidden by the jet radiation. The bottom panel illustrates the case of a BL Lac object, in which the broad lines are not produced because of the very weak radiation produced by the disk (that likely is in the inefficient ADAF regime). We compare the spectrum of 0040–0915 with a well known BL Lac object, PKS 2155–304, as it would be seen if it were at $z = 4.98$. Note that the radio emission of PKS 2155–304 (if it were at $z = 4.98$) is consistent with the upper limit and that the overall energetics and type of spectrum are similar. Both in this and in the “blue quasar” interpretations, the problem is the very poor agreement with the IR-optical data. For comparison, the SED of QSO is reported (orange dashed line, Richards et al. 2006). Black dots are from *Spitzer* IR (Lane et al. 2011).

tangled magnetic field B and moving with a bulk Lorentz factor Γ at a viewing angle θ_v . Throughout the source, relativistic electrons are injected isotropically in the rest frame with a power P'_e as measured in the comoving frame. They are injected with a smoothly joining broken power law, with a break at a random Lorentz factor γ_b , up to the maximum random Lorentz factor γ_{max} . They produce synchrotron and inverse Compton radiation. The seed photons for scattering are the ones produced internally to the jet, by the synchrotron process, and the ones produced externally to the jet, by the accretion disk, its X-ray corona, the BLR, and the torus. The jet power is in the form of produced radiation (P_r), Poynting flux (P_B), kinetic energy of the emitting electrons (P_e), and protons (P_p), assumed to be cold and one per each emitting electron.

We remark that our aim in reproducing the SED of the source is not to find out the exact values of the parameters but,

² From ASDC: <http://www.asdc.asi.it>, SDSS and *Spitzer* (see Lane et al. 2011).

using typical values for the parameters (see, e.g. Ghisellini et al. 2010), to check the consistency of the different classifications.

4.1. The Radio-quiet Quasar Scenario

Figure 4 shows the spectrum produced by a disk around a black hole of mass $M_{\text{BH}} = 1.9 \times 10^9 M_{\odot}$ accreting at 45% of the Eddington rate. This interpretation is consistent with the existing data, considering that the emission of the torus (contributing to the IR luminosity) is rather uncertain. We can then interpret 0040–0915 as a radio-quiet quasar, with a large black hole mass and accreting vigorously. However, unlike other quasars with similar accretion rates and black hole masses, in 0040–0915 there is no (or very weak) broad emission line region. The SED in Figure 4 shows that there is no deficit of ionizing photons, so the absence of the BLR must be caused by something else.

4.2. The Radio-loud Scenarios

An alternative possibility is to detect the source in deep radio band observation with flux just below the current upper limit. In fact, in this case, the source would be characterized by a radio loudness $R_L \geq 15$, that, according to the classical definition by Kellermann et al. (1989), allows us to classify the source as radio loud. This, however, opens up the possibility of two subcases: (1) the jet non-thermal continuum contributes to the optical-UV emission partly swamping the emission lines or (2) the jet is intrinsically weak or misaligned and therefore does not contribute to the optical-UV continuum. In the latter case, this does not solve the problem of weak emission lines, as for the radio-quiet case. Therefore, we concentrate on the first case presenting two canonical examples.

4.2.1. The Blue FSRQ Scenario

We next investigate the case of an FSRQ with a jet pointing at us and emitting a non-thermal spectrum able to hide the lines, of normal luminosities. This requires that the jet continuum also hides the radiation produced by the accretion disk. To have an estimate or upper limit to the disk emission in this case, we have used our IR-optical spectrum to derive an upper limit of the Ly α and C IV broad lines, resulting in $L_{\text{Ly}\alpha} \lesssim 1.1 \times 10^{45} \text{ erg s}^{-1}$ and $L_{\text{C IV}} < 7 \times 10^{44} \text{ erg s}^{-1}$. Assuming the template in Francis et al. (1991; see also Vanden Berk et al. 2001), we can derive an upper limit for the disk luminosity of $L_d < 6 \times 10^{46} \text{ erg s}^{-1}$. Note that our IR-optical spectrum and archival data correspond to a luminosity exceeding $10^{47} \text{ erg s}^{-1}$. The main difficulty of this scenario is the very poor fit to the optical (i.e., rest frame UV) data, severely underestimated. The blue appearance of the jet continuum is achieved by assuming that the dissipation region R_{diss} of the jet is beyond the broad line region R_{BLR} . This implies a deficit of seed photons (produced externally to the jet) that would otherwise rapidly cool the emitting electrons, shifting their relevant energies toward smaller values, and thus producing a redder spectrum (i.e., a synchrotron flux peaking in the sub-millimeter, and a Inverse Compton flux peaking at ~ 10 MeV, as is the case for “normal” FSRQ (see, e.g., Ghisellini & Tavecchio 2015).

4.2.2. The BL Lacertae Scenario

A second possibility to account for a moderate radio-loud source without strong emission lines, is that the source is a BL Lacertae object as tentatively classified by Plotkin et al. (2010). If 0040–0915 is a BL Lac object, then the disk emission would be negligible, and the absence of ionizing photons would be the cause of the absence of the broad emission lines. The entire emission would be produced by the jet. As can be seen in Figures 4 and 5, the main difficulty with this interpretation is the poor fit to the optical data and the infrared *Spitzer* data (Lane et al. 2011), as in the blue FSRQ case. The location of the emitting region is not constrained to be beyond the BLR, but the jet parameters of this case are very similar to the blue FSRQ. The bottom panel of Figure 5 shows also the comparison of the SED of 0040–0915 with the SED of PKS 2155–304, if the latter had $z = 4.98$. We can see that the current radio upper limit is not severe enough to exclude the BL Lac interpretation, but future deeper radio observations can help to discriminate.

In conclusion, our modeling, which combines optical and multi-wavelength data with three possible scenarios, cannot rule out the possibility that this source is indeed a BL Lac object or a blue FSRQ. A critical point in this interpretation is that we expect a radio emission with a flux slightly below the current upper limit. Therefore, we cannot yet establish without any doubt the classification of 0040–0915, and deeper radio observations are mandatory. From the optical point of view, a monitoring of the source could reveal variability or flares expected from non-thermal dominated sources. The newly presented SED prefers the idea that the optical emission is dominated by the direct emission from an accretion disk as expected from a normal QSO. The low luminosity of the lines is puzzling and makes 0040–0915 an example of high-redshift WELQ as discussed by many authors in the literature (see, e.g., Diamond-Stanic et al. 2009).

In order to speculate a little bit more on this final interpretation, we try to accommodate the observed source in the model framework recently drawn in Wu et al. (2012) and Luo et al. (2015) and further discussed with medium resolution optical observation of WELQ by Plotkin et al. (2015) with ESO-XSHOOTER. According to the proposed model (see the sketch in Figure 18 of Luo et al. 2015) the accretion disk of WELQ is geometrically thick and significantly puffed due to the high accretion rate (see also Shemmer et al. 2010). The puffed portion of the disk blocks X-Rays and the ionizing continuum, produced in the nucleus, from reaching the broad line region, resulting in the observed weak line emission. Various scenarios for WELQ (also for their X-Ray properties) can therefore be explained by varying the angle of view as clearly depicted in Luo et al. (2015). In the case of 0040–0915, the X-Ray data seems to be consistent (see Figure 5) with those of normal quasars ($\sim 10^{45} \text{ erg cm}^{-2} \text{ s}^{-1} \text{ \AA}^{-1}$, see, e.g., Maccaro et al. 1991). According to Figure 9 in Wu et al. (2012) and Figure 18 in Luo et al. (2015), when the source is viewed through the shielding gas coming from the puffed disk the X-Ray luminosity is significantly dimmed. Otherwise, a weak-line quasar with X-ray normal luminosity is seen. In the case of 0040–0915, the X-Ray flux does not appear to be absorbed, suggesting that the source is viewed far away from the shielding gas.

We thank the anonymous referee for a careful review of our manuscript that allowed us to greatly improve the presentation of our work. We are also grateful to Dr. John Telting and all the technicians and the astronomers at the Nordic Optical Telescope for support during commissioning and for the acquired observations that this paper refers to. The authors would also like to thank Dr. Thomas Fäcke and Dr. Enrico Orselli (Bayer MaterialScience AG) for providing the custom photopolymeric film for the grating manufacturing. This work was partly supported by the European Community (FP7) through the OPTICON project (Optical Infrared Co-ordination Network for astronomy).

REFERENCES

- Berneth, H., Bruder, F.-K., Fäcke, T., et al. 2013, *Proc. SPIE*, **877603-3**, 8776
- Böttcher, M., & Dermer, C. D. 2002, *ApJ*, **564**, 86
- Calderone, G., Ghisellini, G., Colpi, M., & Dotti, M. 2013, *MNRAS*, **431**, 210
- Cavaliere, A., & D’Elia, V. 2002, *ApJ*, **571**, 226
- Collinge, M. J., Strauss, M. A., Hall, P. B., et al. 2005, *AJ*, **129**, 2542
- Diamond-Stanic, A. M., Fan, Xiaohui., Brandt, W. N., et al. 2009, *ApJ*, **699**, 782
- Fan, X., Strauss, M. A., Richards, G. T., et al. 2006, *AJ*, **131**, 1203
- Farina, E. P., Falomo, R., Decarli, R., Treves, A., & Kotilainen, J. K. 2013, *MNRAS*, **429**, 1267
- Francis, P. J., Hewett, P. C., Foltz, C. B., et al. 1991, *ApJ*, **373**, 465
- Ghisellini, G., & Madau, P. 1996, *MNRAS*, **280**, 67G
- Ghisellini, G., & Tavecchio, F. 2009, *MNRAS*, **397**, 985
- Ghisellini, G., & Tavecchio, F. 2015, *MNRAS*, **448**, 1060
- Ghisellini, G., Tavecchio, F., Foschini, L., et al. 2012, *MNRAS*, **425**, 1371
- Ghisellini, G., Tavecchio, F., Foschini, L., & Ghirlanda, G. 2011, *MNRAS*, **414**, 2674
- Giommi, P., Colafrancesco, S., Padovani, P., et al. 2009, *A&A*, **508**, 107G
- Giommi, P., Padovani, P., Polenta, G., et al. 2012, *MNRAS*, **420**, 2899G
- Kellermann, K. I., Sramek, R., Schmidt, M., Shaffer, D. B., & Green, R. 1989, *AJ*, **98**, 1195
- Landoni, M., Falomo, R., Treves, A., et al. 2013, *AJ*, **145**, 114L
- Landoni, M., Falomo, R., Treves, A., & Sbarufatti, B. 2015, *A&A*, **570**, 126
- Lane, R. A., Shemmer, O., Diamond-Stanic, A. M., et al. 2011, *ApJ*, **743**, 163
- Leipski, C., Meisenheimer, K., Walter, F., et al. 2014, *ApJ*, **785**, 154
- Luo, B., Brandt, W., Hall, P. B., et al. 2015, *ApJ*, **805**, 122
- Maccararo, T., della Ceca, R., Gioia, I. M., et al. 1991, *ApJ*, **374**, 117
- Maraschi, L., Ghisellini, G., Della Ceca, R., & Tavecchio, F. 2010, *ASPC*, **427**, M22
- Meusinger, H., & Balafkan, N. 2014, *A&A*, **568**, A114
- Padovani, P., Giommi, P., Landt, H., & Perlman, E. S. 2007, *ApJ*, **662**, 182P
- Peterson, B. M. 1997, *An Introduction to Active Galactic Nuclei* (Cambridge, New York: Cambridge Univ. Press)
- Plotkin, R. M., Anderson, S. F., Brandt, W. N., et al. 2010, *AJ*, **139**, 390P
- Plotkin, R. M., Shemmer, O., Trakhtenbrot, B., Anderson, S. F., & Brandt, W. N. 2015, *ApJ*, **805**, 123
- Prochaska, J. X., Hennawi, J. F., & Herbert-Fort, S. 2008, *ApJ*, **675**, 1002
- Rector, T. A., Stocke, J. T., Perlman, E. S., Morris, S. L., & Gioia, I. M. 2000, *AJ*, **120**, 1626R
- Richards, G. T., Lacy, M., Storrie-Lombardi, L. J., et al. 2006, *ApJSS*, **166**, 470
- Sbarufatti, B., Treves, A., Falomo, R., et al. 2006, *AJ*, **129**, 559S
- Schneider, D. P., Hartig, G. F., Jannuzi, B. T., et al. 1993, *ApJSS*, **87**, 45
- Shakura, N. I., & Sunjaev, R. A. 1973, *A&A*, **24**, 337
- Shaw, M. S., Romani, R. W., Cotter, G., Healey, S. E., & Michelson, P. F. 2013, *ApJ*, **764**, 135S
- Shemmer, O., Trakhtenbrot, B., Anderson, S. F., et al. 2010, *ApJL*, **722**, L152
- Steidel, C. C., Erb, D. K., Shapley, A. E., et al. 2010, *ApJ*, **717**, 289
- Urry, C. M., & Padovani, P. 1995, *PASP*, **107**, 803
- Vanden Berk, D. E., Richards, G. T., Bauer, A., et al. 2001, *AJ*, **122**, 549
- Wu, J., Brandt, W. N., Anderson, S. F., et al. 2012, *ApJ*, **747**, 10
- Zanutta, A., Bianco, A., Insausti, M., & Garzón, F. 2014b, *Proc. SPIE*, **91515X-1**, 9151
- Zanutta, A., Landoni, M., Bianco, A., et al. 2014a, *PASP*, **264**, 126